Hindawi
International Journal of Energy Research
Volume 2024, Article ID 6628332, 17 pages
https://doi.org/10.1155/2024/6628332

Research Article

Numerical Investigation of Performance Enhancement for Thermoelectric Generator System Optimization of HX Fin Shape

Junbeom Park,[1] **Seongbin Hong**,[1] **Kikon Kwak**,[2] **and Jae-Ho Jeong**[1]

[1]*Mechanical Engineering, Gachon University, Seongnam-si, 1342, Republic of Korea*
[2]*Samsung Heavy Industries, Seongnam-si, 13486, Republic of Korea*

Correspondence should be addressed to Jae-Ho Jeong; jaeho.jeong@gachon.ac.kr

Received 28 November 2023; Revised 12 March 2024; Accepted 13 March 2024; Published 3 April 2024

Academic Editor: Geng Chen

This paper presents a performance analysis and optimization of heat exchanger fin shapes in a thermoelectric power generation system for ship waste heat recovery. It proposes a new curved fin design aimed at enhancing heat transfer efficiency and maximizing thermoelectric power generation capacity. Numerical analysis and response surface methodology (RSM) focused on 225 parameters to identify the optimal fin shape. Computational analysis using CFX was conducted on the thermoelectric module system with curved fins. The methodology was verified by comparing and analyzing CFD and PIV experimental results for a curved fin. The paper comprehensively compares the fluid dynamics of curved fins and straight fins, highlighting how curved fins improve heat exchange by creating a tip leak vortex. The results demonstrate the superiority of the curved fin design in terms of heat transfer efficiency and net power generation over the conventional straight fin design.

1. Introduction

The growth of the world economy has led to increased industrialization and international trade. Large volumes of raw materials, fuels, and finished products are transported daily over vast distances by land, air, and ocean [1]. The combustion of fossil fuels to power this movement of goods has led to enormous emissions of greenhouse gases. GHG (greenhouse gas) emissions have adverse effects on the climate, environment, and public health [2, 3]. The emission of GHG has led to the formation of surface ozone and an increase of particulate matter (PM) in the atmosphere, which adversely affects public health. In recent years, the number of cases of chronic respiratory diseases has increased globally [4]. Furthermore, global temperatures have significantly increased due to the global warming effect of GHG. This has led to changes in climate patterns and extreme weather conditions, destroying a wide range of ecosystems and natural habitats. The Intergovernmental Panel on Climate Change (IPCC) has proposed that the global temperature rise be curbed to 1.5°C compared to preindustrial levels by 2100 to prevent catastrophic climate change [5, 6]. In the short term, however, we must achieve carbon neutrality by the year 2050.

Among the many sources of GHG emissions, maritime transport has received some of the least attention, yet it is also a major contributor [2, 3, 7]. Due to its high energy efficiency compared to other modes of transportation, shipping is responsible for more than 80% of global trade and contributes about 1-3% of the world's gross domestic product (GDP) [8]. However, it accounts for approximately 2-4% of GHG emissions, which is projected to increase by approximately 250% by 2050 based on existing scenarios [5, 7–9]. This contrasts sharply with the target of reducing greenhouse gas emissions by 50-85% by 2050, which is required to keep global temperature rise below 1.5°C [2, 9]. The main GHG emitted by ships is carbon dioxide (CO_2) which has a global warming potential of 98% [5, 7, 10]. The effects of other non-CO_2 GHG emitted from ships have also been assessed [3]. The International Maritime Organization (IMO), a body that regulates shipping, is strongly enforcing environmental regulations on CO_2 emissions around the world, to reduce the emissions by 50% by the year 2050 [5]. By applying the Energy Efficiency Design Index (EEDI),

newly built ships are forced to improve their energy efficiency by 10% compared to the baseline in 2015, 20% compared to the baseline in 2020, and 30% compared to the baseline in 2025. In addition, due to the strengthened regulation, the Energy Efficiency Existing Ship Index (EEXI) will be applied at the same level as EEDI for existing ships that were not subject to regulation by 2026 [6, 9]. On the sea, the practice of slow steaming in which the general sailing speed is reduced has been widely adopted for GHG emissions during shipment. Slow steaming decreases fuel consumption thereby decreasing the CO_2 emissions and fuel expenses [9]. However, due to delays in the delivery time, slow steaming may lead to increased logistic costs or increased CO_2 emission levels in comparison to land transportation [8]. Other measures for CO_2 reductions in shipping include the use of alternative fuels such as LNG, renewable energy sources (such as kites and solar cells), and waste heat recovery for power generation [1, 9, 11, 12]. Eide et al. [2] analyzed the cost-effectiveness of several technical and operational measures for reducing CO_2 emissions from shipping for selected ships and found that these measures were viable and should be pursued.

The energy efficiency of shipping is essential for the reduction of global energy demands and GHG emissions, as less fuel is consumed [13, 14]. Significant amounts of residual heat are contained in the exhaust of the main engine of ships. The fuel efficiency of modern diesel engines is usually about 48–51% [11, 15–17]. The remaining amount of the input energy is usually lost as waste heat contained in the exhaust gas and jacket water that is discharged into the atmosphere. Although there is a considerable amount of wasted energy in the exhaust gases, its quality is usually low due to its low temperature and limited potential for power production [18]. The waste heat released by the main engine is usually used to heat heavy fuel oil and accommodation areas and to generate fresh water, which decreases its temperature to a level too low for optimal use [19]. However, this energy, and the high-quality waste heat from the waste incinerator exhaust, can be turned into electrical power with high-efficiency value using waste heat recovery systems such as thermoelectric generators (TEGs) [20]. This can greatly increase the energy efficiency and sustainability of the shipping industry [11, 15, 18, 21]. Converting all forms of waste heat into useful power will not only improve fuel consumption but also reduce CO_2 and other harmful exhaust emissions. TEG is one of the most promising technologies for energy recovery from low- and medium-temperature waste heat [14]. Compared to other methods, the TEG system can convert thermal energy into electrical energy without moving parts or chemical reactions. It has the advantage of low noise, low maintenance cost, and high safety, being able to be applied without limitation, and does not incur much cost for maintenance or repair a long life span [16, 19, 20]. The thermoelectric power generator system is used to recover 40% of waste heat loss from the main engine to improve the efficiency of the ship.

A TEG is a solid-state device that generates electrical power directly from a temperature gradient. It is a type of thermoelectric device that converts heat energy into electrical energy without any moving parts or combustion processes which eliminates extra costs resulting from maintenance and replacement [11, 14, 21, 22]. TEGs are based on the thermoelectric (or Seebeck) effect, which is the generation of an electric voltage or current in a thermoelectric material when subjected to a temperature difference. This effect was discovered in 1821 by Thomas Johann Seebeck, and it occurs due to the diffusion of charge carriers (electrons or holes) in response to a temperature gradient [14, 18, 23]. When two dissimilar conductors are joined together to form a thermocouple, an electric voltage is generated that is proportional to the temperature difference between the two ends of the thermocouple. The thermocouples are connected electrically in series and thermally in parallel in a thermoelectric module (TEM) that is designed to maximize the voltage output and minimize the thermal losses. TEGs are typically made of semiconductor materials, such as bismuth telluride, lead telluride, or silicon-germanium, which have high thermoelectric efficiency and can operate at relatively low temperatures [24]. The operating principle of a TEG is relatively simple. When one side of the TEM is heated and the other side is cooled, a temperature gradient is established across the module, which generates an electric voltage across each thermocouple. The voltage outputs from all the thermocouples are connected in series to produce a higher voltage output. The efficiency of a TEG is determined by its thermoelectric figure of merit (ZT), which is a measure of the material's ability to convert heat into electricity [25]. ZT is defined as $ZT = (\alpha^2 \sigma T)/\kappa$, where α is the Seebeck coefficient, σ is the electrical conductivity, T is the absolute temperature, and κ is the thermal conductivity. A higher ZT value corresponds to a higher conversion efficiency and a higher power output [15, 23]. Improving the performance of the heat exchanger is necessary to maximize the amount of thermoelectric power generation [26, 27].

As a prior study to improve the heat exchanger performance of the TEG system, research was conducted on the presence or absence of the shape of fins. According to a study conducted by Chen et al., it was confirmed that the performance of TEM using 78 square fins was improved by 24.14% compared to using plate fins [28]. According to a study conducted by Garud et al., the performance of a heat exchanger with inclined fins was confirmed to improve overall efficiency by 1.88% and power generation by 35% compared to a straight fin heat exchanger [29]. According to the research conducted by Quan et al., optimizing the internal structure of the heat exchanger through a new study with blade-shaped fins resulted in a 15.8% improvement in output. Furthermore, it was confirmed that the height of the fins has the most significant impact on the TEG system, emphasizing the importance of optimizing temperature, pressure drop, and output [30, 31]. Much research has been conducted on not only the shape of the fin but also the placement of the fin [32, 33]. In this way, improving the performance of thermoelectric power generation systems according to fins is very important research being actively conducted.

In this study, the heat transfer performance of heat exchanger fins was compared by changing design variables through numerical analysis, and the optimal design was derived using RSM (response surface methodology). Due

to the nature of the ship system, the TEG internal structure was optimized to increase power generation through sufficient waste heat absorption within a limited space. Improving heat transfer within a limited space can be achieved through forced convection or the generation of vortex flow; however, forced convection requires a new power source, and vortex generators increase the pressure drop [23]. Ma et al. [34] applied a longitudinal vortex generator to the TEG exhaust heat exchange channel and compared it with the smooth channel. The total power output was increased by a maximum of 153%. In this study, the shape of the thermocouple fins was optimized to generate vortex flow with the element and conditions for lower pressure drop investigated. This will not only improve the heat transfer area but also improve the convective heat transfer performance and cut the hard layer to increase heat absorption. This study introduces novel perspectives previously unaddressed in the literature, particularly through detailed analysis of the structure and scale of vortices generated by fin shapes using vortex core identification. By doing so, it offers deeper insights into optimizing fin designs for improved heat transfer and fluid dynamics in the field.

2. Numerical Analysis Methodology

2.1. Computational Geometry Model and Curved Fin Design Parameter. The schematic shown in Figure 1 illustrates a finned thermoelectric power generator system. The high-temperature fluid flows through the upper part of the module, while the coolant flows through the lower part, forming a heat exchanger system that supplies heat to the thermoelectric power generator system. The heat exchanger has a width of 288 mm and a length of 414 mm, with a duct size of 288 ∗ 21 mm. The thermoelectric power generator system consists of a total of nine fin-attached thermoelectric modules, as depicted in Figure 2. Information regarding the design parameters of the fins can be found in Figure 2 and Table 1. The thermoelectric module has a height of 10 mm and is composed of eight fins, including four reference fins and four height-variable fins.

The heat transfer performance of 225 cases (comprising 5 heights, 5 radii of curvature, 3 fin pitches, and 3 boundary conditions) was analyzed using ANSYS CFX.

2.2. CFD Methodology Validation. To validate the accuracy of the numerical analysis methodology employed in this study, particle visualization experiments using the proposed curved fin were conducted and compared with the computational analysis results. This comparison served to confirm the consistency between the numerical model's accuracy and the observed experimental outcomes, thereby establishing the validity of the proposed numerical analysis methodology.

2.2.1. PIV Experiment Apparatus. The particle image velocimetry (PIV) method is utilized experimentally to scrutinize the attributes of the flow field, averaged over time, by introducing tracer particles into the fluid flow and leveraging the images acquired via laser illumination. This approach stands as a pivotal instrument in the realm of fluid dynamic research, extensively employed for the visual scrutiny and analysis of fluid motion and flow [35].

In this paper, experiments were conducted using a particle image velocimetry (PIV) setup, which comprises components such as a seeding generator, test section, camera, laser, and a fan. Specifically, 1 μm-sized olive oil particles were employed, and image data were acquired using a camera with a resolution of 2, 048 ∗ 2,048 pixels, utilizing the PIV-630076 model. The experiment utilized a PIV-MGL-N-2.5 W laser with a wavelength of 532 nm and an output of 2.5 W. The experimental apparatus is shown in Figure 3.

2.2.2. Test Section and Data Measurement Location. The test section, composed of acrylic measuring 170 mm × 170 mm × 360 mm, was used to illustrate the shape of the curved fin employed in the experiments and the positions for data measurement, as depicted in Figure 4. The configuration of the curved fin designated the downstream positions as 4 mm, 14 mm, and 24 mm, referred to as positions 1, 2, and 3, respectively. Comparative analysis was conducted between the flow visualization results at seven points for each position and the computational fluid dynamic (CFD) results.

2.2.3. Comparison of PIV and CFD Results. The boundary conditions utilized in the experiments and computational analysis are presented in Table 2. The inlet velocity is 5 m/s, while the inlet temperature is 293.15 K. Furthermore, the turbulent model employed for computational analysis is SST, with a total of three million structured grids utilized for numerical simulations. The normalized velocity fields obtained from the experimental results and computational analysis are depicted in Figure 5, confirming the similarities in the streamlines and flow patterns between the experiment and the computational analysis.

Moreover, quantitative data is compared and analyzed in Figure 6, revealing an average deviation of approximately 11% at position 1, around 9% at position 2, and approximately 16% at position 3. The consistency in the results of both the experiment and the computational analysis across all positions validates the adequacy of the numerical analysis methodology employed in this study. This serves to affirm that the adopted computational approach effectively reproduces the fluid dynamic phenomena. Thus, the study provides evidence that the selected computational analysis method sufficiently replicates the fluid dynamic phenomena.

2.3. Grid Sensitivity Analysis. To ensure the accuracy and reliability of computational fluid dynamic (CFD) results in the thermoelectric power generator system, grid independence analysis was conducted. The pressure drop was used as the criterion to evaluate the grid independence of the CFD results, as shown in Figure 7. The analysis revealed that when the number of mesh cells exceeded 10 million, the error of the pressure drop was less than 1%. This indicates that the CFD results are independent of the mesh resolution when the number of mesh cells is greater than 10 million. Based on this finding, the CFD domain was constructed using 10 million mesh cells, as shown in Figure 8. By

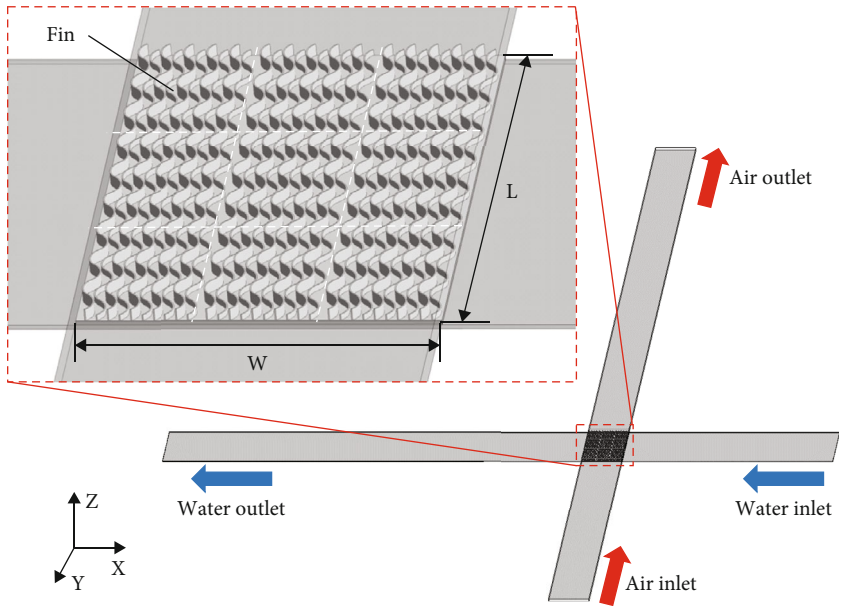

Figure 1: Schematics of thermoelectric power generator system.

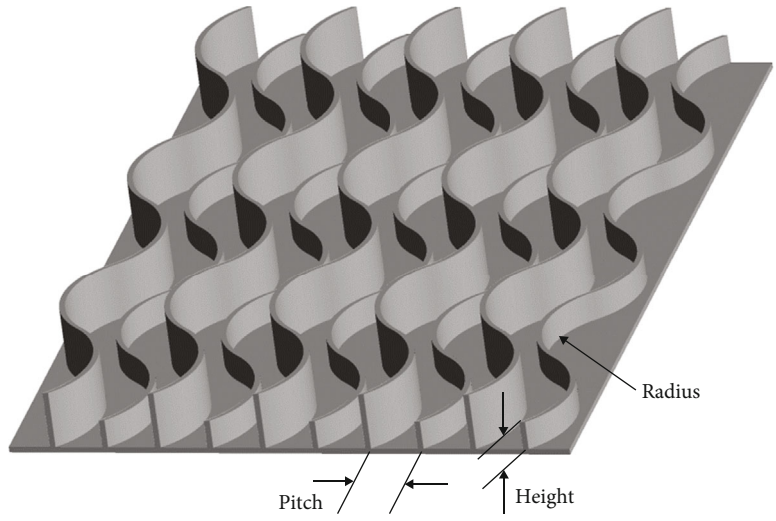

Figure 2: Geometry parameter of the curved fin with a height difference.

Table 1: Description of CFD analysis variables.

Parameter	Value
Fin pitch	8, 10, 12
Height	5, 6, 7, 8, 10
Radius	15, 17, 20, 25, 30
Reynolds number	107,000~210,000

employing a grid of this size, the CFD simulation could provide accurate and reliable results for the thermoelectric power generator system. The use of such a fine mesh ensures that the numerical solution is consistent with the physical reality, enabling the investigation of detailed flow features and heat transfer characteristics. Consequently, the analysis and results obtained from this study can be trusted for designing and optimizing the thermoelectric power generator system.

2.4. Computational Analysis Boundary Condition. The domain and boundary conditions of the fin-attached thermoelectric module used in the analysis are shown in Figure 9 and Table 3. As a high heat source for the high-temperature part of the thermoelectric module, air at 200 degrees flows. The phenomenon according to the flow rate was analyzed for these three flow rate conditions. Cooling water at 20 degrees flows as a low heat source in the low-temperature part of the thermoelectric module.

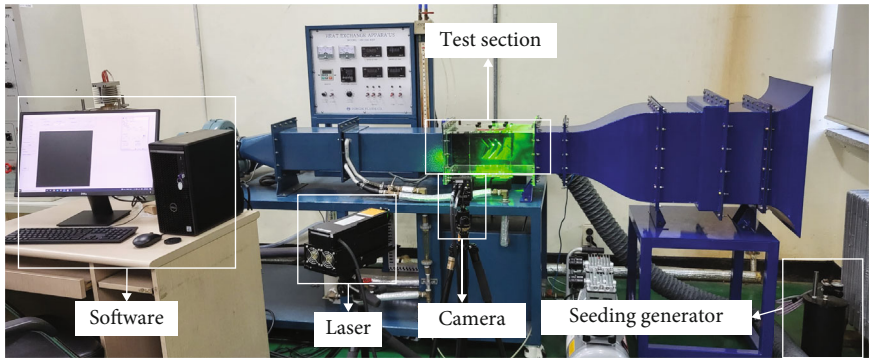

Figure 3: Particle image velocimetry experiment apparatus.

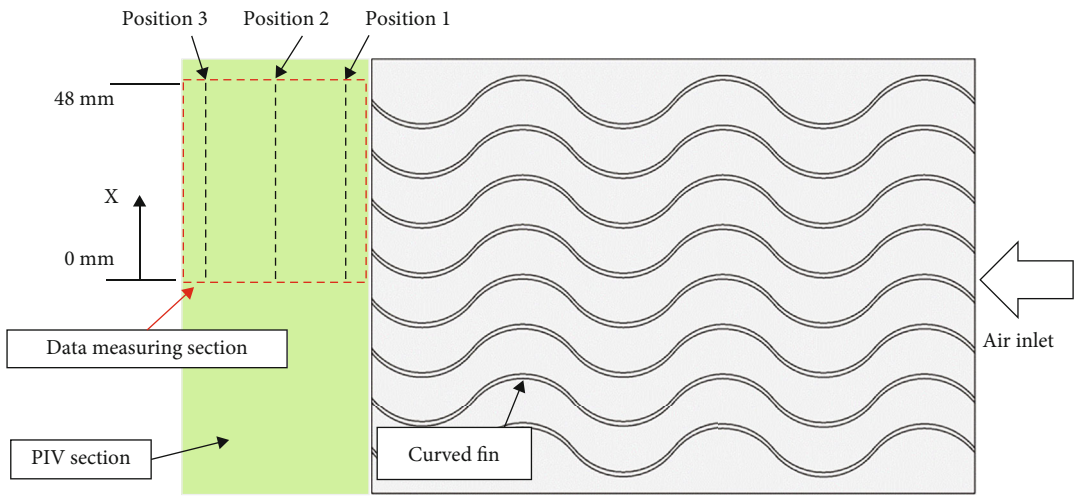

Figure 4: PIV section and measuring position.

Table 2: Boundary conditions for PIV experiments and CFD.

Parameter	Experiment value (unit)	CFD value (unit)
Inlet velocity	5 (m/s)	5 (m/s)
Inlet temperature	293.15 (K)	293.15 (K)
Turbulence model	—	SST
Number of mesh	—	3,000,000

The SST model was used for the turbulence model, and the computational grid system was constructed by using a hexahedral mesh. To construct a computational grid system, $y+$ was set under 1. The upper and lower parts of the thermoelectric module and fins were set with copper, and the thermal conductivity of the semiconductor part of the module was set at 0.1 W/mK.

2.5. Governing Equation and Power Generation Correlation. SST $k-w$ turbulence models are commonly used in computational fluid dynamics to simulate the effects of turbulence and heat transfer. These models are based on the Reynolds-averaged Navier-Stokes (RANS) equations, which describe the motion of a compressible fluid.

In the case of simulating heat transfer through a tube, the fluid is assumed to be incompressible and the tube is assumed to be insulating. The dominant equations of the continuous equation, the momentum equation, and the energy equation are solved simultaneously to determine the fluid flow and temperature distribution in the tube.

By solving these equations simultaneously using SST $k-w$ turbulence models, it is possible to accurately simulate the flow and temperature distribution in a tube and predict the heat transfer rate between the fluid and the tube wall. This type of analysis is commonly used in the design and optimization of heat exchangers, which are critical components in many industrial processes [36].

Continuity equation:

$$\frac{\partial \rho}{\partial t} + \nabla \bullet (\rho U) = 0. \tag{1}$$

Momentum equations:

$$\frac{\partial (\rho U)}{\partial t} + \nabla \bullet (\rho U \otimes U) = -\nabla p + \nabla \bullet \tau + S_{\mathrm{M}}, \tag{2}$$

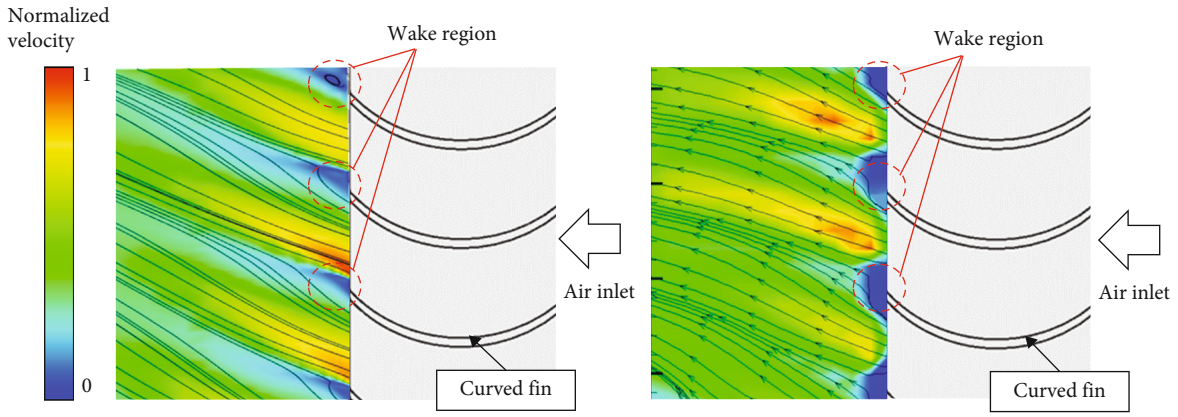

(a) CFD analysis results (b) PIV experimental results

Figure 5: CFD and PIV test-normalized velocity results.

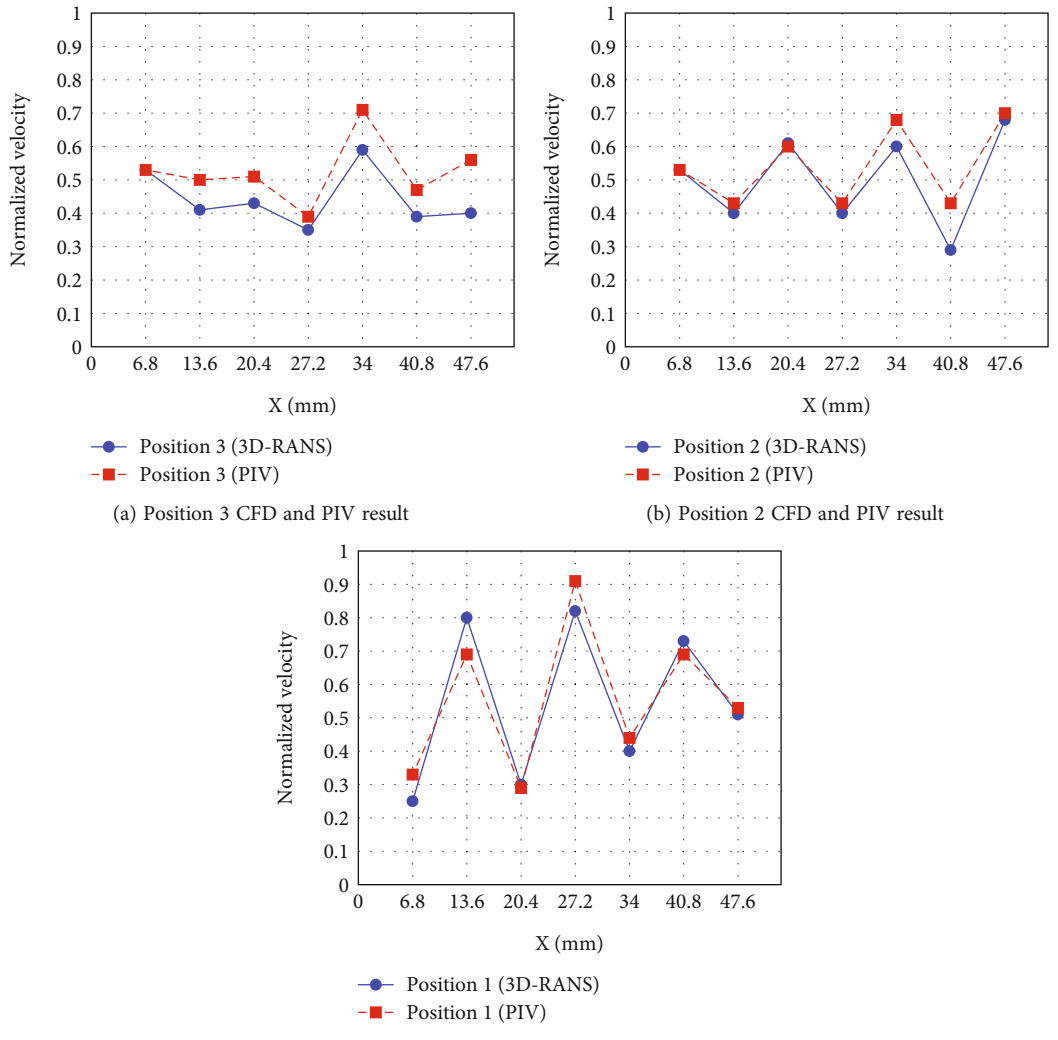

(a) Position 3 CFD and PIV result

(b) Position 2 CFD and PIV result

(c) Position 1 CFD and PIV result

Figure 6: Comparison of PIV and CFD results by position.

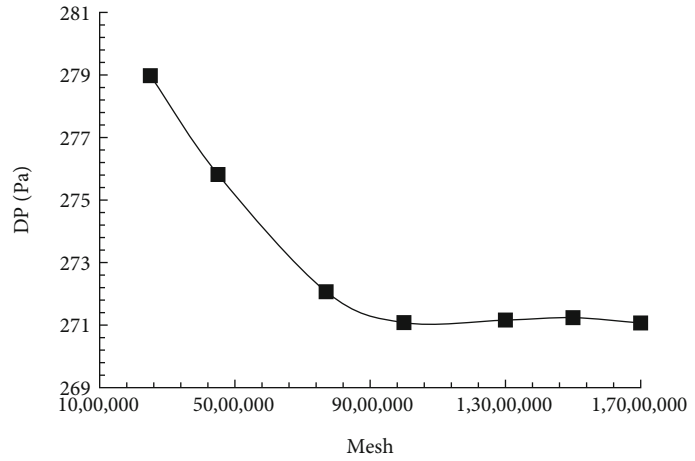

Figure 7: Mesh sensitivity analysis according to pressure drop.

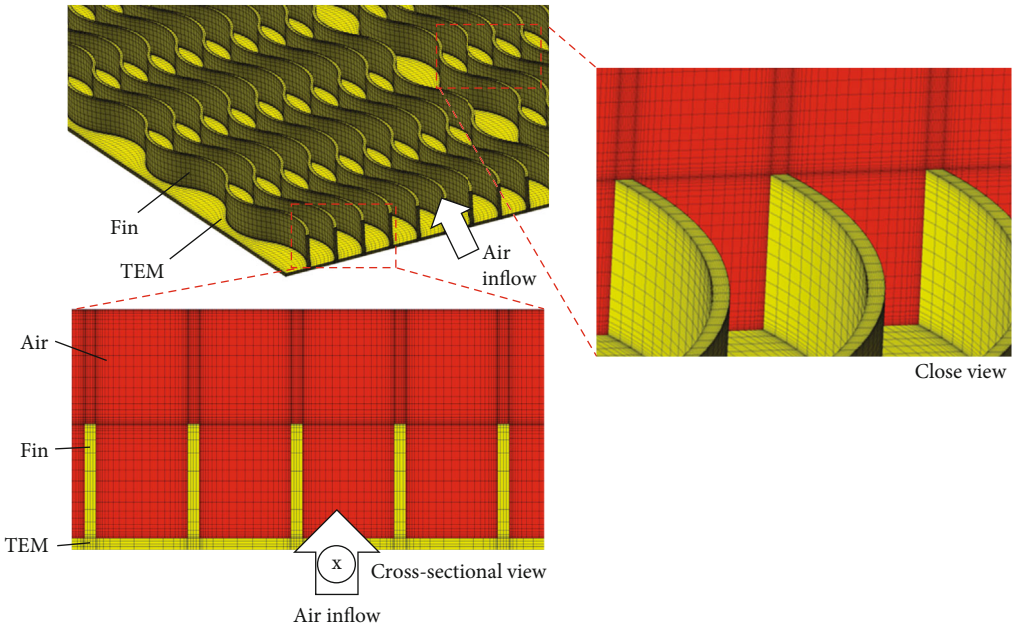

Figure 8: The computational grid system of thermoelectric power generator system.

where τ is the stress tensor defined by

$$\tau = \mu\left(\nabla U + (\nabla U)^{\mathrm{T}} - \frac{2}{3}\,\delta\nabla\bullet U\right). \tag{3}$$

Total energy equation:

$$\frac{\partial(\rho\, h_{\mathrm{tot}})}{\partial t} - \frac{\partial p}{\partial t} + \nabla\bullet(\rho\, U\, h_{\mathrm{tot}}) = \nabla\bullet(\lambda\nabla T) + \nabla\bullet(U\bullet\tau) + U\bullet S_{\mathrm{M}} + S_{\mathrm{E}}, \tag{4}$$

where h_{tot} is the stress tensor defined by

$$h_{\mathrm{tot}} = h + \frac{1}{2}\,U^2. \tag{5}$$

The power generated by the thermoelectric power generation system is defined as follows.

$$P_{\mathrm{TEG}} = n \times \left\{\frac{\alpha \times (T_{\mathrm{h}} - T_{\mathrm{c}})}{R_{\mathrm{TEG}} + R_{\mathrm{L}}}\right\}^2 \times R_{\mathrm{L}}. \tag{6}$$

P_{TEG} is the amount of power generation of the thermoelectric power generation system, n is the number of thermoelectric modules, α is the Seebeck coefficient, T_{h} is the temperature of the high-temperature part of the thermoelectric module, T_{c} is the temperature of the low temperature of the thermoelectric module, R_{TEG} is the electrical resistance of the thermoelectric generator, and R_{L} is the internal resistance.

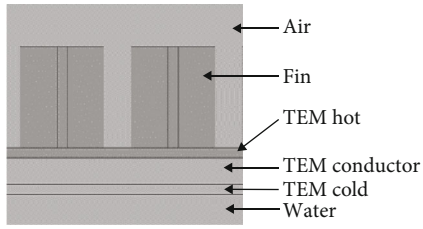

Figure 9: Cross-sectional view of thermoelectric module.

Table 3: Boundary condition for CFD.

Parameter	Value
$y+$	<1
Turbulence model	SST
Air inlet temperature	200°C
Air inlet Reynolds number	107,000~210,000
Water inlet temperature	20°C
Fin, TEM hot, TEM cold	Copper
TEM conductor conductivity	0.1 W/mK

The power generation loss due to the pressure drop in the thermoelectric power generation system is defined as follows.

$$P_{\text{loss}} = \Delta P \times \dot{V}. \tag{7}$$

P_{loss} is the power generation loss of the thermoelectric power generator system, ΔP is the pressure drop, and $\dot{V}$ is the volumetric flow rate.

The net power generation amount considering the pressure drop of the thermoelectric power generation system is defined as follows [28].

$$P_{\text{net}} = P_{\text{TEG}} - P_{\text{loss}}. \tag{8}$$

The efficiency of TEG system is defined as follows [37].

$$\eta = \frac{P_{\text{TEG}}}{Q_{\text{h}}} = \frac{P_{\text{TEG}}}{\dot{m}_{\text{h}} C_{\text{h}} \Delta T_{\text{h}}}, \tag{9}$$

where $\dot{m}_{\text{h}}$, C_{h}, and ΔT_{h} are the mass flow rate, specific heat capacity, and temperature difference between the air inlet and outlet.

2.6. Vortex Identification Methodology. In this study, the vortex core identification methodology developed by Sawada was utilized [38]. This methodology bears resemblance to Perry and Chong's critical point theory [39], but it assumes that a local flow velocity field can be linearized within a tetrahedral cell, distinguishing it from conventional vortex identification methodologies. The linearization of the local velocity field enables the streamline equation to be analytically integrable within the cell, allowing for the determination of potential vortex cores.

In order to analyze complex three-dimensional flow fields, normalized helicity was employed in conjunction with the aforementioned vortex core identification technique. The normalized helicity can be defined as outlined in [40].

$$H_n = \frac{\vec{\zeta} \bullet \vec{v}}{\left|\vec{\zeta}\right| \bullet \left|\vec{v}\right|}. \tag{10}$$

$\vec{\zeta}$ and $\vec{v}$ represent absolute vorticity and velocity, respectively. This value can be obtained from -1 to 1. By the value, normalized helicity represents physical meaning as follows.

Negative: vortex rotates by left-hand rule with streamwise.

Zero: vortex stagnates.

Positive: vortex rotates by right-hand rule with streamwise.

By coloring visualized vortex core using normalized helicity, complicate three-dimensional flow field that occurs in curved fin analyzed.

3. CFD Results and Discussion

3.1. Flow Characteristics. In this section, a detailed comparison and analysis of the flow phenomenon caused by the curved fin and the widely used straight fin was undertaken. Through this investigation, the aim was to gain a better understanding of the differences between the two types of fins and to identify the key factors that affect their performance.

To achieve this, a series of simulations and visualizations were used to examine the vorticity and vortex structure of both curved and straight fins. The results of this analysis are presented in Figure 10, which highlights the temperature and vortex structure of each type of fin through normalized helicity visualization.

The normalized helicity visualization clearly shows that no vortices are present in the straight fins, whereas the curved fins exhibit distinct tip leakage vortexes. Furthermore, the system with curved fins exhibits significantly enhanced heat exchange compared to the system with straight fins, as confirmed through temperature field analysis. The curved shape of the fins induces a change in flow direction and creates vortex structures, resulting in increased heat transfer. This phenomenon can be visually observed through temperature distributions, demonstrating the crucial role of curved fins in improving heat exchange efficiency. Thus, the application of curved fins proves to be a beneficial strategy for enhancing heat transfer and overall heat exchange efficiency.

Overall, the analysis suggests that the curved fin has a more complex flow structure than the straight fin and that the presence of the tip leakage vortex may be a key factor contributing to the differences in performance between the two types of fins. These findings have important implications for the design and optimization of fin-based heat exchangers and other related systems.

The aim of this study is to investigate the fluid dynamics involved in the flow over a curved fin, with a particular focus on the pressure fields, streamlines, vortex structures, and

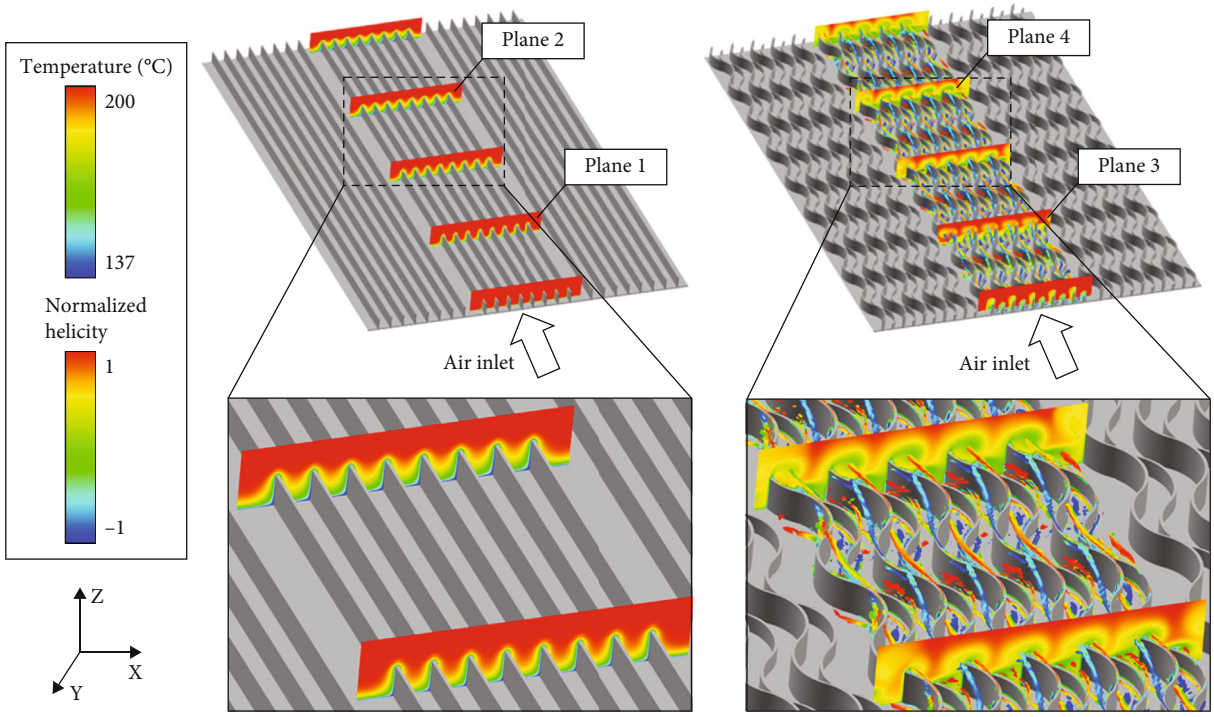

Figure 10: Temperature distributions and vortex structure of (a) straight and (b) curved fin.

vorticity associated with planes 3 and 4 as illustrated in Figure 10. Detailed analysis and interpretation of the curved fin was conducted to provide valuable insights into the subject matter. Figure 11 represents a cross-section of the curve bent to the right of plane 3 and Figure 12 a cross-section of a curve bent to the left of plane 4 of the curved fin in Figure 10.

Figures 11(a) and 12(a) depict the adherence of the fluid to the curved surface as the fin bends at plane 3 and plane 4, respectively. Notably, the concave region acts as the suction surface, driven by the Coanda effect, while the convex part creates a pressure surface, resulting in a significant pressure difference. This pressure disparity gives rise to a range of intriguing phenomena, secondary flow, and tip leakage vortex deserving our attention and scrutiny.

Closer examination of planes 3 and 4 is shown in Figures 11(b) and 12(b). It is more evident that the fluid flow along the curve of the fin experiences separation at the inflection point of the curve. This separation is predominantly influenced by the pressure exerted by the suction surface, leading to the formation of a captivating phenomenon known as the tip leakage vortex. The presence of this vortex can be observed through the temperature field, where it induces a longitudinal vortex that facilitates heat exchange with the upper part of the air, which is not in direct contact with the fin. The interplay between the main flow and the secondary flow gives rise to a complex flow pattern that significantly impacts the overall fluid dynamics.

Further analysis of plane 3 and plane 4 in Figures 11(c) and 12(c) unveils an intriguing observation regarding the directionality of the tip leakage vortex induced by the Coanda effect. In plane 3, it is established that the tip leakage vortices manifest in the direction aligned with the primary flow. These vortices, characterized by swirling motion at the tip of the curved fin, arise due to the interaction between the main flow and the secondary flow. On the other hand, unlike in plane 3, the tip leakage vortices in plane 4 emerged in the opposite direction to that of the main flow. This finding suggests that the direction of the tip leakage vortex periodically changes in accordance with the bending direction of the curved fin. Consequently, the intricate fluid dynamics surrounding the curved fin are profoundly influenced by the fin's bending direction, leading to a captivating interplay between the fluid flow and the system's geometry.

Furthermore, the separated flow generated by the fin has been shown to have a significant impact on the thermal performance of the fin. The reduction in the boundary layer thickness due to the separated flow has been observed to reduce the temperature gradient across the fin, resulting in a more uniform temperature distribution along the fin surface.

As a result, the mixing effect of the flow can be maximized, which in turn improves the heat transfer performance.

3.2. Heat Transfer Characteristics. The curved fin serves a crucial function in improving heat absorption through increased heat transfer area and turbulent flow. The geometrical parameters of the curved fin play a significant role in determining the degree of turbulence generated and the reduction of boundary layer thickness. The effectiveness of the curved fin in achieving optimal heat transfer depends on the ability of designers to optimize these parameters. By

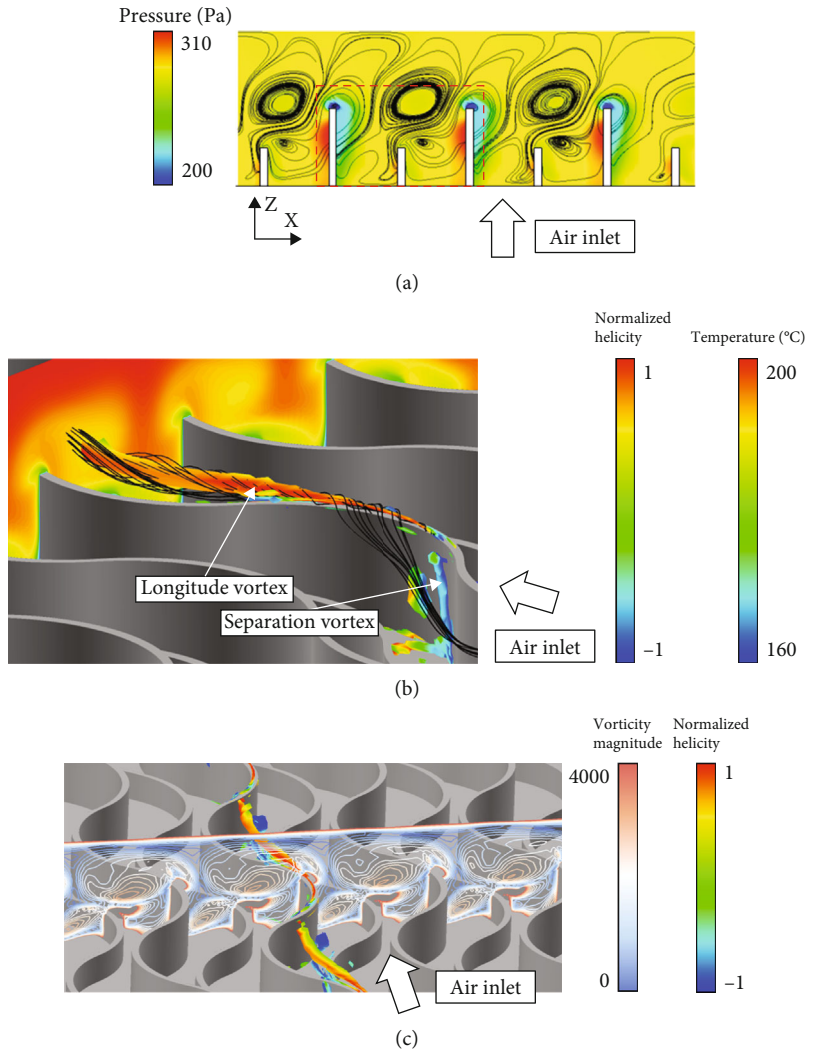

Figure 11: Cross-section plane 3 of the curved fin in Figure 10. (a) Pressure field with cross-sectionally projected streamline, (b) vortex core and temperature field, and (c) vortex core and vorticity field.

optimizing these parameters, designers can ensure that the curved fin operates at maximum efficiency, thereby enhancing its overall heat transfer capabilities.

The temperature field for the cross-section shown in Figure 10 was further analyzed to gain a better understanding of the heat transfer performance of the fin. The results of this analysis are presented in Figure 13.

In the temperature field of Figure 13(c), corresponding to a curved fin at plane 3, it can be observed that heat exchange takes place even at the top of the air that is not directly in contact with the fin. Additionally, the thickness of the boundary layer in this case is observed to be thin. In contrast, in the temperature field of Figure 13(a), which corresponds to a straight fin at plane 1, it can be observed that the heat exchange does not occur at the top of the air and the boundary layer is thick.

When the temperature field at the rear of the fin, where the flow is fully developed, is compared, it is observed in the case of Figure 13(d) (plane 4 of curved fin) that the mixing effect is maximized due to the presence of a tip leakage vortex and heat exchange with the upper part of the air is uniform. This results in a more efficient heat transfer process. On the other hand, the temperature field in Figure 13(b) (plane 2 of curved fin) indicates that the thickness of the boundary layer becomes thicker and the heat exchange performance deteriorates as a result.

These observations demonstrate that the geometry of the fin, specifically the curvature of the fin and the presence of a tip leakage vortex, plays a critical role in determining the heat transfer performance. The presence of a curved fin and a tip leakage vortex results in a more efficient heat transfer process due to the reduction of the boundary layer thickness and the increased mixing of the fluid. In contrast, a straight fin without a vortex leads to a thicker boundary layer and reduced heat transfer performance.

Figure 14 presents the temperature graph of the high-temperature region of the thermoelectric module, showcasing a numerical comparison of the heat transfer performance between the curved fin and the straight fin. The position in the axial direction of the system is used to

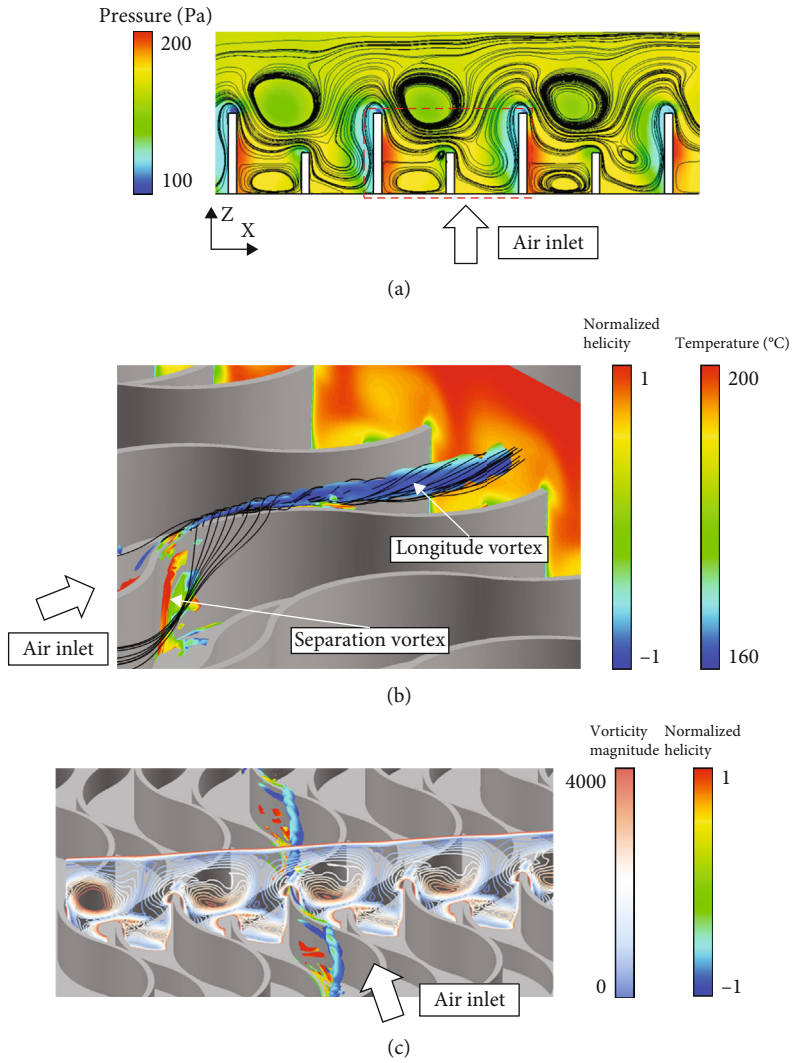

Figure 12: Cross-section plane 4 of the curved fin in Figure 10. (a) Pressure field with cross-sectionally projected streamline, (b) vortex core and temperature field, and (c) vortex core and vorticity field.

evaluate the heat transfer performance based on the flow characteristics. The temperature of the high-temperature region in the thermoelectric module is a crucial parameter used to calculate the power generated through thermoelectric power generation and serves as an indicator of the heat exchange response.

In the analysis, the curved fin with the highest performance at a flow Reynolds of 107,000 was employed. The temperature of the high-temperature region at the initial position, corresponding to 10% of the axial direction, exhibited a 5.2% improvement in the curved fin compared to the straight fin. As the flow progressed, it was observed that the temperature difference between the curved fin and the straight fin in the high-temperature region increased. Notably, at the rear end, specifically at 90% of the axial direction, the temperature improvement reached 11.5%. This numerical analysis provides an explanation for this phenomenon by elucidating that the rotation direction of the longitudinal vortex, which is a characteristic flow pattern of the curved fin, periodically changes according to the direction of the curve. This periodic variation maximizes the mixing effect, leading to enhanced heat transfer and temperature improvement in the high-temperature region.

These findings highlight the superior heat transfer performance of the curved fin compared to the straight fin, emphasizing the significant impact of the curved fin's flow characteristics on the temperature distribution within the thermoelectric module.

3.2.1. Effect of Radius of Curvature. In this study, response surface methodology (RSM) was employed to analyze the performance concerning the shape variables of fins. The aim was to understand the impact of small fin height and curvature radius of the fin on performance across different pitches and Reynolds numbers.

Figures 15 and 16 represent the outcomes obtained through RSM. RSM visualizes the relationship between two input variables (radius of curvature and fin height) and

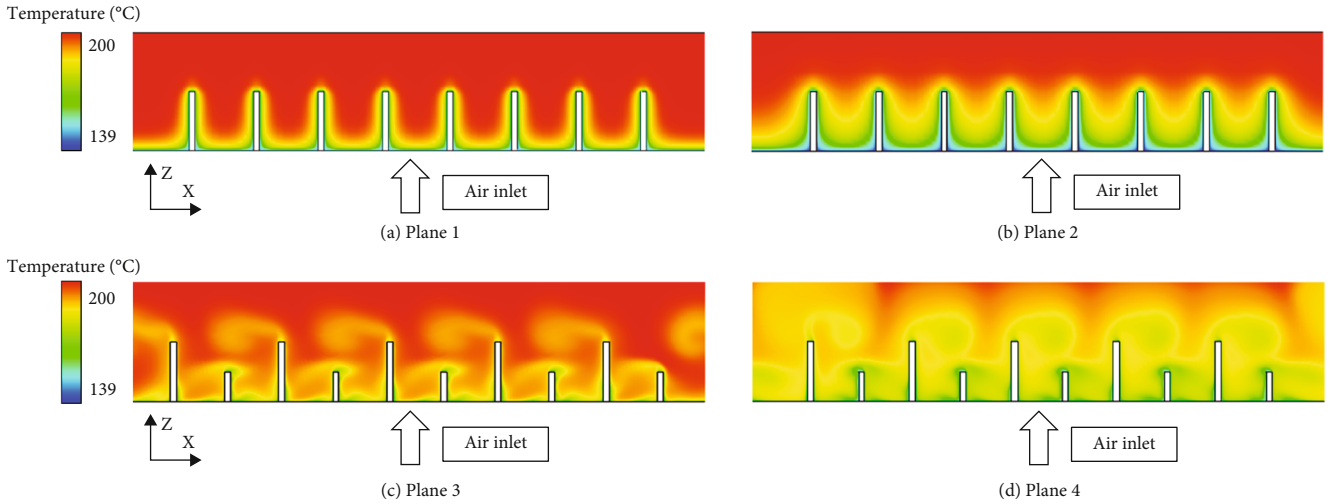

Figure 13: Temperature contours (a, b) of the straight fin at planes 1 and 2 and (c, d) of the curved fin at planes 3 and 4.

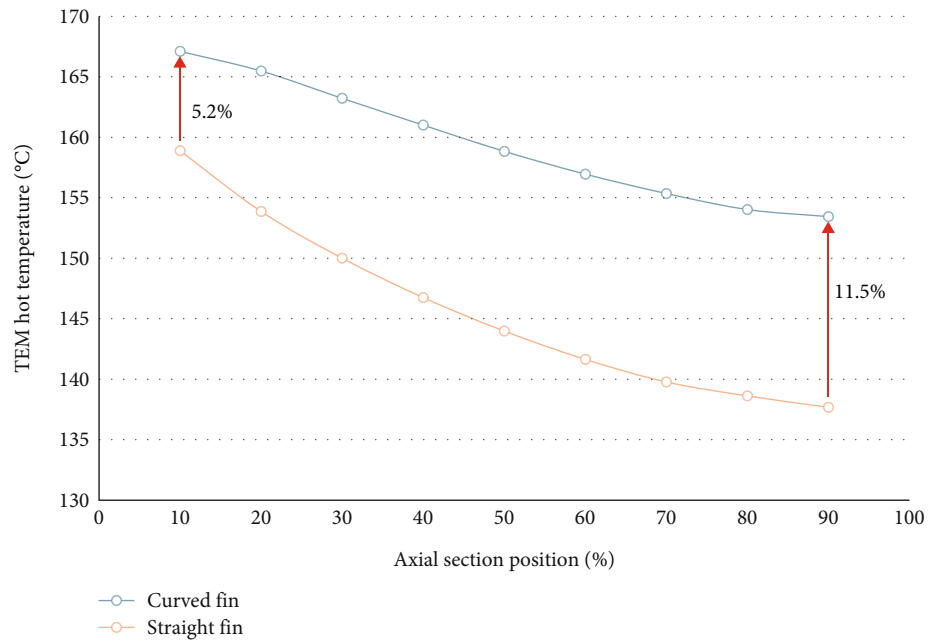

Figure 14: Numerical comparison of the heat transfer performance between curved fin and straight fin.

response variables (Nu and net power) via three-dimensional graphs or surfaces. This visualization facilitates the comprehension of interactions between each input variable and aids in identifying optimal conditions.

The graphs depict the values of Nu (heat transfer coefficient) and net power with respect to the variables radius and height. The color gradient, where red signifies higher values and blue lower ones, offers a visual insight into the impact of these variables on performance.

These findings quantitatively elucidate the influence of fin shape variables on heat transfer and fluid dynamic characteristics, aiding in determining optimal conditions. Through RSM, a comprehensive understanding of complex interactions led to the derivation of an optimal design.

The results of the study are shown in Figure 15, which plots the Nusselt number against the radius of curvature and fin height for different Reynolds number and pitches. The graph confirms that the Nusselt number increases as the radius of curvature decreases, indicating that smaller radii lead to greater turbulence and improved heat transfer. This trend is observed for all pitches, small fin heights, and Reynolds number parameters. The increase in the Nusselt number can be attributed to the impact of the vortex created by the pressure difference caused by the fin's curvature.

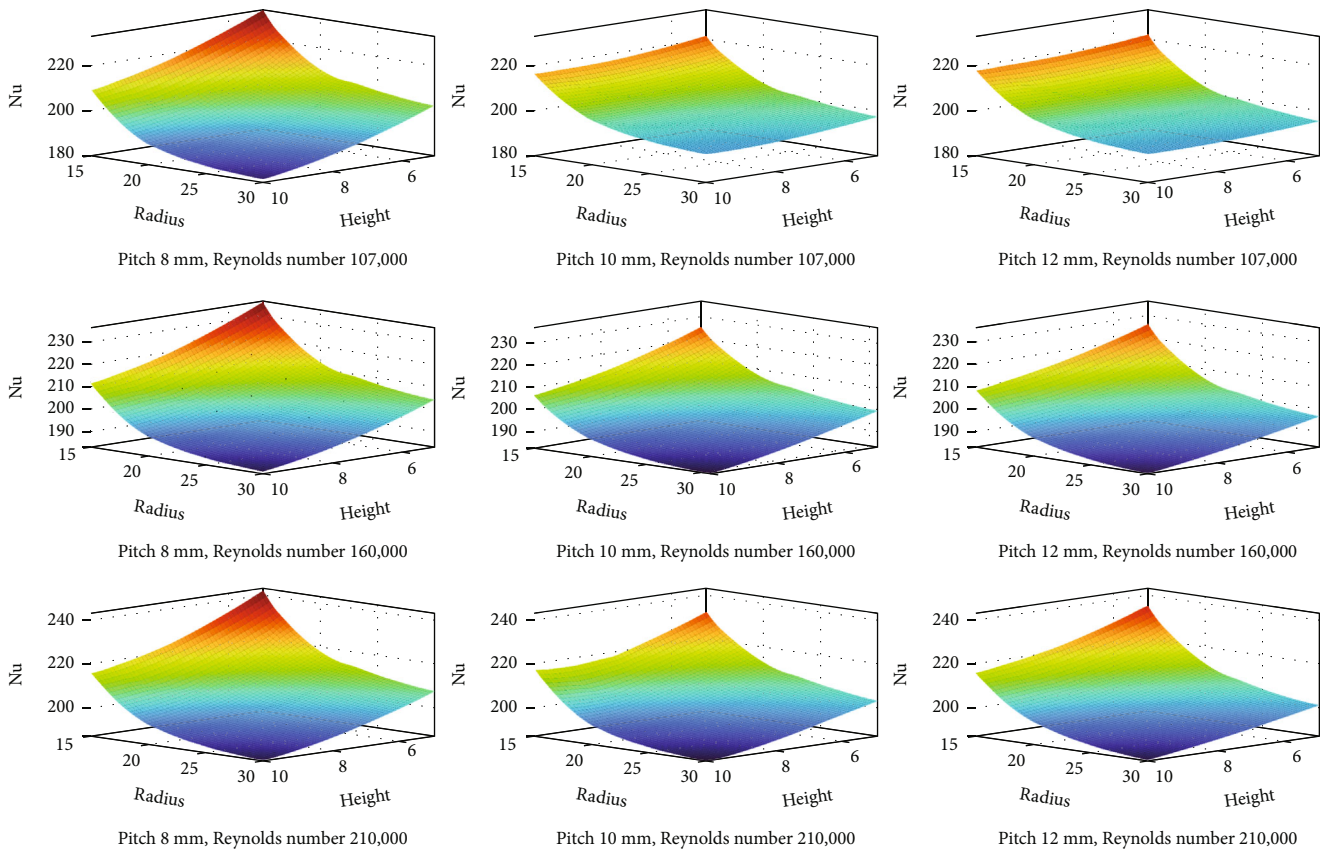

Figure 15: Response surface plot by 225 cases about the Nusselt number.

These findings suggest that the geometrical parameters of the curved fin have a significant impact on its heat transfer capabilities.

3.2.2. Effect of Fin Height. The change in the number of Nusselt according to the height of the small fin is shown in Figure 15 as well. The graph reveals that the Nusselt number increases as the height of the small fin decreases. This results in the reduction of the boundary layer on the fin's surface, thereby enhancing the heat transfer performance. The curvature of the fin generates a secondary flow that passes over the small fin, creating a larger secondary flow. This, in turn, reduces the thickness of the boundary layer and improves heat transfer. Thus, the findings of the study indicate that the small fin's height is a crucial parameter that affects the heat transfer characteristics of the system.

3.2.3. Effect of Fin Pitch. Figure 15 shows the variation in the Nusselt number with respect to fin pitch. Unlike the radius of curvature and small fin height parameters, it can be observed that the trend of the Nusselt number changes with fin pitch. Specifically, fin pitch 8 mm resulted in a high Nusselt number, while pitches 10 mm and 12 mm produced similar values of the Nusselt number. In contrast to the aforementioned parameters, the trend of the Nusselt number varied as the radius of curvature and fin height increased or decreased. Our findings indicate that the optimal fin pitch is 8 mm, and the effect of pitch on performance is relatively small compared to the impact of radius of curvature and height.

3.3. Power Generation Performance. In a thermoelectric power generation system, improving the heat exchange performance by utilizing fin of a heat exchanger is crucial. The previous section analyzed and optimized the flow and heat transfer characteristics based on fin shape. However, the allowable pressure in the exhaust system of a ship limits the optimization of fin shape. Thus, this section focuses on optimizing the fin shape within the allowable pressure range. The optimization is based on the amount of power generated through the temperature difference at both ends of the device and the net amount of power generation, considering the P loss due to pressure drop.

Response surface methodology (RSM) was used to analyze the net power generation from 225 cases and is presented in Figure 16. Tables 4–6 present the performance of the optimized curved fin and the straight fin at each Reynolds number, respectively.

The results of the study indicate that for a Reynolds number of 107,000, cases with smaller radii of curvature and lower heights of the height-variable fin result in higher net power.

The optimal fin shape based on the net power generation at a Reynolds number of 107,000 has a pitch of 8 mm, a radius of curvature of 15 mm, and a variable fin height of 5 mm, confirming that the heat transfer characteristics are

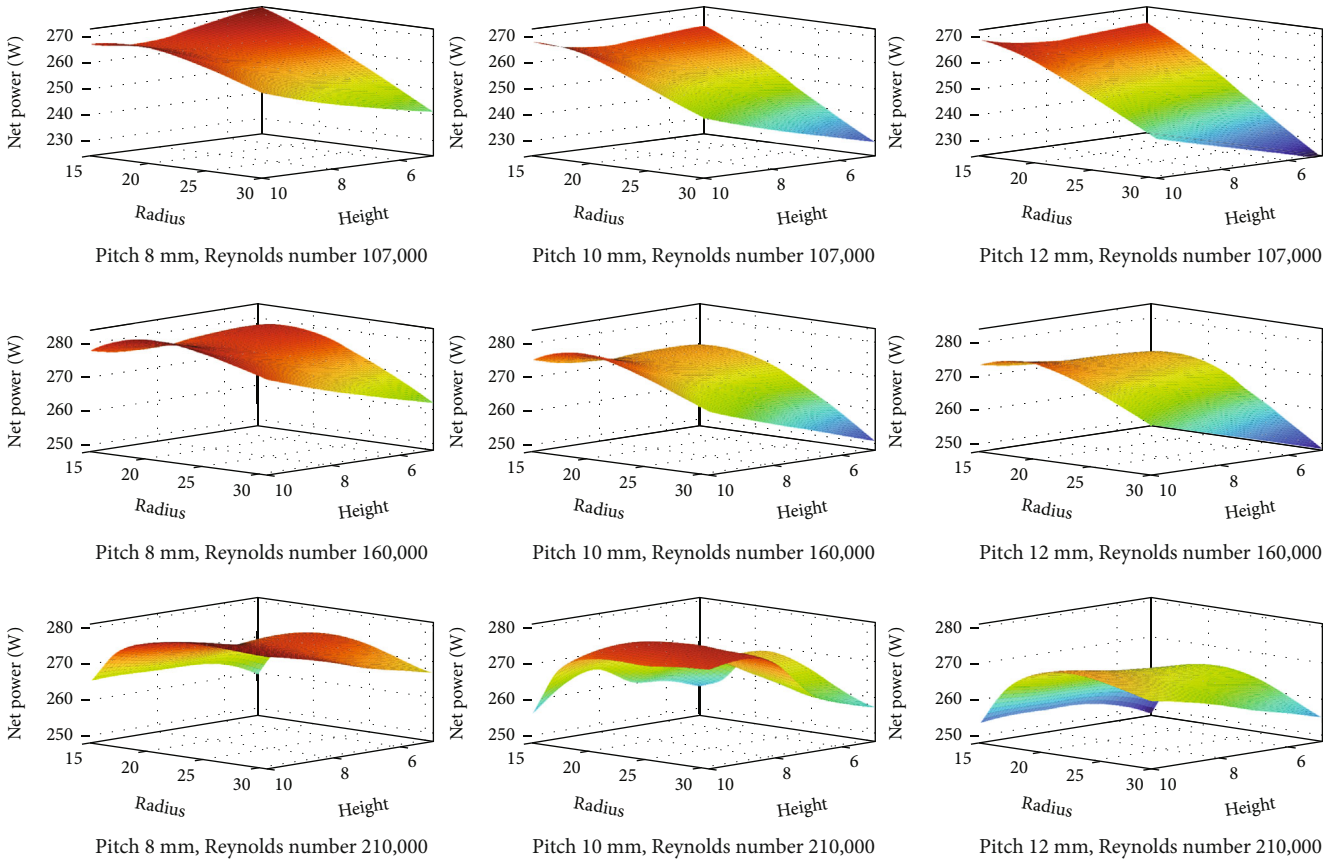

Figure 16: Response surface plot by 225 cases about net power.

Table 4: Best performance of curved fin and straight fin results at the Reynolds number 107,000.

Cases	DT (°C)	Power (W)	DP (Pa)	P loss (W)	Net power (W)	η (%)
P8-H5-R15	138.6	296.8	402.3	24.3	272.5	0.33
Straight	122.8	240.9	194.9	11.8	229.1	0.27

Table 5: Best performance of curved fin and straight fin results at the Reynolds number 160,000.

Cases	DT (°C)	Power (W)	DP (Pa)	P loss (W)	Net power (W)	η (%)
P8-H10-R20	145.4	321.7	631.8	38.2	283.5	0.36
Straight	133.4	277.9	395.5	23.9	254	0.31

the same as the best shape. When comparing the net power generation of a fin with a radius of curvature of 15 mm and a variable fin height of 10 mm, which has similar heat transfer performance, and a fin with a radius of curvature of 30 mm and a variable fin height of 5 mm, the difference in the value is large. Loss due to pressure drop occurs due to the difference in power. The highest net power generation was 272.2 W, which is about 20% higher than the lowest power generation of 224 W. A detailed comparison between the curved fin and the straight fin, specifically focusing on their performance in terms of net power generation, is presented in Table 4. The net power generation of the optimized curved fin demonstrates a significant improvement of approximately 19% when compared to the straight fin.

For a Reynolds number of 160,000, the highest power generation occurred when the radius of curvature was about 20 mm and the height of the height-variable fin was 9 to 10 mm. This shows an optimal shape different from the shapes with the highest heat transfer characteristics, such as a curvature radius of 15 mm and a variable fin height of 5 mm. It was confirmed that the optimum shape was different because the flow rate increased and the power loss due to the pressure drop increased rather than the increase in power generation through heat transfer characteristics. The

Table 6: Best performance of curved fin and straight fin results at the Reynolds number 210,000.

Cases	DT (°C)	Power (W)	DP (Pa)	P loss (W)	Net power (W)	η (%)
P8-H10-R20	149.4	336.3	931	56.3	280	0.38
Straight	140.2	302.4	656.4	39.7	262.7	0.34

shape with the highest power generation has a pitch of 8 mm, a radius of curvature of 20 mm, and a variable in height of 10 mm, with a power generation of 283.5 W. The power generation improved by approximately 11% compared to the lowest power generation of 248 W. The net power generation of the optimized curved fin demonstrates a significant improvement of approximately 11.6% when compared to the straight fin.

At a Reynolds number of 210,000, the highest amount of power generation occurred when the radius of curvature was about 25 mm and the height of the variable height fin was 10 mm, and the net power amount was 281 W. The power generation improved by approximately 8.8% compared to the lowest power generation of 249 W. The net power generation of the optimized curved fin demonstrates a significant improvement of approximately 6.5% when compared to the straight fin.

The results of the study indicate that the optimal conditions for maximizing power generation varied depending on the Reynolds number of the flow, radius of curvature, height, and fin pitch of the height-variable fin. In this study, it was found that the net power generation trend in this section was different from the Nusselt number trend observed in the previous section depending on the fin shape. An increase in the Nusselt number led to an improvement in heat transfer performance, resulting from an increase in turbulence generated by the fins. However, this improvement was accompanied by the observation of large pressure drops, which resulted in significant power losses. Additionally, it was confirmed that the power loss due to the pressure drop increased as the flow rate increased, leading to varying trends in net power generation at different flow rates. These findings emphasize the importance of optimizing the fin shape not only based on heat transfer properties but also on net power generation. Thus, to achieve maximum net power generation, it is crucial to consider both heat transfer performance and pressure drop.

By understanding the optimal conditions for generating the highest net power, this research may have important implications for the development of more efficient TEG system.

4. Conclusion

This thesis focused on the design, optimization, and performance analysis of a thermoelectric power generator (TEG) fin for waste heat recovery in the maritime industry. Through detailed numerical analysis and simulations, the performance of curved fins in the TEG heat exchanger was compared to straight fins. The performance of the optimal curved fin was observed to improve by 19%, 11.6%, and 6.5% compared to the straight fin at the Reynolds numbers 107,000, 160,000, and 210,000, respectively. The results demonstrated that the curved fin design significantly improved heat exchange efficiency, leading to enhanced power generation. The presence of tip leakage vortices induced by the Coanda effect in curved fins played a vital role in the improved heat transfer performance. The findings shed light on the importance of optimizing fin geometries to achieve maximum heat exchange and power generation.

Furthermore, the thesis employed response surface methodology (RSM) to optimize the fin shape for net power generation, considering both heat transfer characteristics and pressure drop. The research demonstrated that achieving the highest net power generation required a careful balance between heat transfer performance and pressure drop to avoid excessive power losses.

The performance of the proposed curved fins varies significantly with changes in flow velocity, necessitating the determination of an optimal shape that suits the fluid dynamics. Applying such curved fins to thermoelectric power generation systems requires considering suitable configurations and optimal placements based on their positions. Moreover, there is a need for further research to understand how the performance of these fins is influenced by their locations concerning the varying flow velocities. Through this research, a deeper comprehension of the optimal configuration and enhanced performance of curved fins in thermoelectric power generation systems is anticipated to be attained.

While the research focused on thermoelectric power generation systems for ship waste heat recovery, the discoveries stemming from the curved fin design are transferable to various fields utilizing air as a high-temperature heat source in thermoelectric power generation systems. Moreover, the insights gained from this study might find applicability not only in thermoelectric systems but also in designing fins for heat exchangers. The revelations concerning heat transfer and fluid dynamics through curved fins can be applied broadly across flow conditions in heat exchange processes. These findings extend beyond the current scope of research, offering a profound understanding applicable to diverse systems aimed at heat transfer.

Data Availability

The RES file data used to support the findings of this study are available from the corresponding author upon request.

Conflicts of Interest

The authors declare that there is no conflict of interest regarding the publication of this paper.

Acknowledgments

This work was supported by the Korea Institute of Energy Technology Evaluation and Planning (KETEP) grant funded by the Korea government (MOTIE) (2021202080023B (Development and demonstration of thermoelectric power generation system for marine application by waste heat utilization) and RS-2023-00243201 (Global Talent Development project for Advanced SMR Core Computational Analysis Technology Development)).

References

[1] ICCT, *Reducing Greenhouse Gas Emissions from Ships*, ICCT, Washington DC, 2011.

[2] M. S. Eide, Ø. Endresen, R. Skjong, T. Longva, and S. Alvik, "Cost-effectiveness assessment of CO_2 reducing measures in shipping," *Maritime Policy & Management*, vol. 36, no. 4, pp. 367–384, 2009.

[3] M. S. Eide, S. B. Dalsøren, Ø. Endresen et al., "Reducing CO_2 from shipping–do non-CO_2 effects matter?," *Atmospheric Chemistry and Physics*, vol. 13, no. 8, pp. 4183–4201, 2013.

[4] X. Q. Jiang, X. D. Mei, and D. Feng, "Air pollution and chronic airway diseases: what should people know and do?," *Journal of Thoracic Disease*, vol. 8, no. 1, pp. E31–E40, 2016.

[5] Ø. Buhaug, J. J. Corbett, Ø. Endresen et al., *Second IMO GHG*, IMO, London, UK, 2009.

[6] T.-H. Joung, S.-G. Kang, J.-K. Lee, and J. Ahn, "The IMO initial strategy for reducing greenhouse gas (GHG) emissions, and its follow-up actions towards 2050," *Journal of International Maritime Safety, Environmental Affairs, and Shipping*, vol. 4, no. 1, pp. 1–7, 2020.

[7] T. W. P. Smith, J. P. Jalkanen, B. A. Anderson et al., *Third IMO GHG Study 2014*, IMO, London, United Kingdom, 2015.

[8] E. Ben-Hakoun, M. Shechter, and Y. Hayuth, "Economic evaluation of the environmental impact of shipping from the perspective of CO_2 emissions," *Journal of Shipping and Trade*, vol. 1, no. 1, p. 5, 2016.

[9] J. V. Fenhann, *CO_2 emissions from international shipping*, vol. 4, APA, 2017.

[10] H. Lindstad, G. S. Eskeland, H. Psaraftis, I. Sandaas, and A. H. Strømman, "Maritime shipping and emissions: a three-layered, damage-based approach," *Ocean Engineering*, vol. 110, Part B, pp. 94–101, 2015.

[11] T. Uyanık, E. Ejder, Y. Arslanoğlu et al., "Thermoelectric generators as an alternative energy source in shipboard microgrids," *Energies*, vol. 15, no. 12, p. 4248, 2022.

[12] T. Ouyang, Z. Wang, G. Wang, Z. Zhao, S. Xie, and X. Li, "Advanced thermo-economic scheme and multi-objective optimization for exploiting the waste heat potentiality of marine natural gas engine," *Energy*, vol. 236, article 121440, 2021.

[13] C. Forman, I. K. Muritala, R. Pardemann, and B. Meyer, "Estimating the global waste heat potential," *Renewable and Sustainable Energy Reviews*, vol. 57, pp. 1568–1579, 2016.

[14] H. Jouhara, A. Żabnieńska-Góra, N. Khordehgah et al., "Thermoelectric generator (TEG) technologies and applications," *International Journal of Thermofluids*, vol. 9, article 100063, 2021.

[15] G. Shu, Y. Liang, H. Wei, H. Tian, J. Zhao, and L. Liu, "A review of waste heat recovery on two-stroke IC engine aboard ships," *Renewable and Sustainable Energy Reviews*, vol. 19, pp. 385–401, 2013.

[16] Z. Su, M. Zhang, P. Xu et al., "Opportunities and strategies for multigrade waste heat utilization in various industries: a recent review," *Energy Conversion and Management*, vol. 229, article 113769, 2021.

[17] A. Mahmoudi, M. Fazli, and M. R. Morad, "A recent review of waste heat recovery by organic Rankine cycle," *Applied Thermal Engineering*, vol. 143, pp. 660–675, 2018.

[18] D. V. Singh and E. Pedersen, "A review of waste heat recovery technologies for maritime applications," *Energy Conversion and Management*, vol. 111, pp. 315–328, 2016.

[19] D. Champier, "Thermoelectric generators: a review of applications," *Energy Conversion and Management*, vol. 140, pp. 167–181, 2017.

[20] N. R. Kristiansen and H. K. Nielsen, "Potential for usage of thermoelectric generators on ships," *Journal of Electronic Materials*, vol. 39, no. 9, pp. 1746–1749, 2010.

[21] N. R. Kristiansen, G. J. Snyder, H. K. Nielsen, and L. Rosendahl, "Waste heat recovery from a marine waste incinerator using a thermoelectric generator," *Journal of Electronic Materials*, vol. 41, no. 6, pp. 1024–1029, 2012.

[22] M. Hamid Elsheikh, D. A. Shnawah, M. F. M. Sabri et al., "A review on thermoelectric renewable energy: principle parameters that affect their performance," *Renewable and Sustainable Energy Reviews*, vol. 30, pp. 337–355, 2014.

[23] R. Aridi, J. Faraj, S. Ali, T. Lemenand, and M. Khaled, "Thermoelectric power generators: state-of-the-art, heat recovery method, and challenges," *Electricity*, vol. 2, no. 3, pp. 359–386, 2021.

[24] J. Pei, B. Cai, H.-L. Zhuang, and J.-F. Li, "Bi_2Te_3-based applied thermoelectric materials: research advances and new challenges," *National Science Review*, vol. 7, no. 12, pp. 1856–1858, 2020.

[25] N. Jaziri, A. Boughamoura, J. Müller, B. Mezghani, F. Tounsi, and M. Ismail, "A comprehensive review of thermoelectric generators: technologies and common applications," *Energy Reports*, vol. 6, pp. 264–287, 2020.

[26] M. Dzida, J. Girtler, and S. Dzida, "On the possible increasing of efficiency of ship power plant with the system combined of marine diesel engine, gas turbine and steam turbine in case of main engine cooperation with the gas turbine fed in series and the steam turbine," *Polish Maritime Research*, vol. 16, no. 3, pp. 26–31, 2009.

[27] F. Meng, L. Chen, Y. Feng, and B. Xiong, "Thermoelectric generator for industrial gas phase waste heat recovery," *Energy*, vol. 135, pp. 83–90, 2017.

[28] W.-H. Chen, C.-M. Wang, L. Huat Saw, A. T. Hoang, and A. A. Bandala, "Performance evaluation and improvement of thermoelectric generators (TEG): fin installation and compromise optimization," *Energy Conversion and Management*, vol. 250, article 114858, 2021.

[29] K. S. Garud, J.-H. Seo, M. S. Patil et al., "Thermal–electrical–structural performances of hot heat exchanger with different internal fins of thermoelectric generator for low power generation application," *Journal of Thermal Analysis and Calorimetry*, vol. 143, no. 1, pp. 387–419, 2021.

[30] R. Quan, J. Wang, W. Liang, X. Li, and Y. Chang, "Numerical investigation of a thermoelectric generator system with embedded sickle-shaped fins," *Applied Thermal Engineering*, vol. 236, article 121741, 2024.

[31] R. Quan, H. Guo, D. Liu, Y. Chang, and H. Wan, "Performance optimization of a thermoelectric generator for automotive application using an improved whale optimization algorithm," *Sustainable Energy & Fuels*, vol. 7, no. 23, pp. 5528–5545, 2023.

[32] Y. Wang, S. Li, X. Xie, Y. Deng, X. Liu, and C. Su, "Performance evaluation of an automotive thermoelectric generator with inserted fins or dimpled-surface hot heat exchanger," *Applied Energy*, vol. 218, pp. 391–401, 2018.

[33] S.-C. Tzeng, T.-M. Jeng, and Y.-L. Lin, "Parametric study of heat-transfer design on the thermoelectric generator system," *International Communications in Heat and Mass Transfer*, vol. 52, pp. 97–105, 2014.

[34] T. Ma, X. Lu, J. Pandit et al., "Numerical study on thermoelectric–hydraulic performance of a thermoelectric power generator with a plate-fin heat exchanger with longitudinal vortex generators," *Applied Energy*, vol. 185, pp. 1343–1354, 2017.

[35] M. Raffel, C. E. Willert, F. Scarano, C. J. Kähler, S. T. Wereley, and J. Kompenhans, *Particle Image Velocimetry: A Practical Guide*, Springer, 2018.

[36] CFX-Solver, ANSYS, *Theory guide. Release ll*, CFX-solver, 2006.

[37] R. Quan, Y. Li, T. Li, Y. Chang, and H. Yan, "Numerical and experimental study on performance of a low-backpressure polyhedral thermoelectric generator for waste heat recovery," *Journal of Thermal Science*, vol. 32, no. 1, pp. 109–124, 2023.

[38] K. Sawada, "A convenient visualization method for identifying vortex centers," *Transactions of the Japan society for Aeronautical and Space Sciences*, vol. 38, no. 120, pp. 102–116, 1995.

[39] A. E. Perry and M. S. Chong, "A description of eddying motions and flow patterns using critical-point concepts," *Annual Review of Fluid Mechanics*, vol. 19, no. 1, pp. 125–155, 1987.

[40] Y. Levy, D. Degani, and A. Seginer, "Graphical visualization of vortical flows by means of helicity," *AIAA Journal*, vol. 28, no. 8, pp. 1347–1352, 1990.